Scientific Research Publishing

International Journal of Geosciences, 2025, 16(8), 505-526
https://www.scirp.org/journal/ijg
ISSN Online: 2156-8367
ISSN Print: 2156-8359

Mineragraphic Studies of Upper Carboniferous—Upper Permian Phosphate Nodules from Chamba Basin of Chamba District, Himachal Pradesh, India

Tariq Masood[1*], Shamim A. Dar[2*], K. Farahim Khan[1]

[1]Department of Geology, Aligarh Muslim University, Aligarh, India
[2]Department of Geology, Institute of Science, Banaras Hindu University, Varanasi, India
Email: *tariq.masood44@gmail.com, *sjshamim@gmail.com

How to cite this paper: Masood, T., Dar, S.A. and Khan, K.F. (2025) Mineragraphic Studies of Upper Carboniferous—Upper Permian Phosphate Nodules from Chamba Basin of Chamba District, Himachal Pradesh, India. *International Journal of Geosciences*, **16**, 505-526.
https://doi.org/10.4236/ijg.2025.168024

Received: June 26, 2025
Accepted: August 9, 2025
Published: August 12, 2025

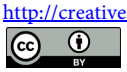

Abstract

Phosphate nodules from the Upper-Carboniferous to Upper-Permian period were discovered in the Chamba District of Himachal Pradesh. They are hosted by the Salooni formation and are sporadically found in black carbonaceous slate. They are grey to black coloured and vary from sub-round to oval shape, often exhibiting sharp conchoidal fractures. The petrography, X-ray diffractometry (XRD), and scanning electron microscopy (SEM) reveal that the phosphate mineral assemblages are dominated by cryptocrystalline apatite, namely collophane (carbonate fluorapatite or CFA) in studied samples. Quartz veins are often found in the nodules, along with associated gangue minerals, including, microcrystalline silica, carbonate and pyrite as minor constituents. The findings of the textural study show that the phosphates are present in both the pelletal form as well as apatite-rich matrix together with microfossil remnants. Clay minerals fillings suggest the intense chemical weathering of continental sources. The outcomes of this study suggest that the variations in the mineral morphologies, texture, and presence of organic matter within the phosphate nodules may be a result of early diagenesis precipitation of Carbonate Fluorapatite (CFA) crystals in the porewater with the help of activity of microorganisms at the sediment-water interface.

Keywords

Carbonate Fluorapatite, Chamba, Microbial Filament, Phosphate Nodule, Salooni Formation

1. Introduction

Phosphorus, though comprising only 0.09 wt.% of Earth's crust [1], is the tenth most abundant element and plays a critical role in both geological and biological processes. Among minerals, phosphates are notably complex and diverse, with around 460 identified species [2]. Phosphorus is essential for the growth and development of all living organisms and serves as a limiting nutrient for marine biological productivity over geological timescales [3]]. While it forms part of certain proteins, its primary biological role lies in forming the structural basis of vertebrate bones and teeth, as well as the shells and chitinous exoskeletons of various invertebrates [4]. Marine sedimentary phosphates represent a major sink for phosphorus (P), a vital element for all life forms [5] [6]. Phosphates existing at the interface of biological and geological systems play a key role in the global phosphorus cycle [7].

Rock phosphate, also known as phosphorite, is a marine biochemical sedimentary rock enriched in phosphorus, typically containing at least 18 wt.% P_2O_5 and in some cases up to 40 wt.%. It is commonly formed in coastal upwelling zones [8]-[12] when specific physical conditions align with biological activity during early diagenesis [7] [13]. Phosphate (PO_4^{3-}) crystallizes into francolite—also known as carbonate-fluorapatite (CFA)—as authigenic cryptocrystalline masses. These phosphatic particles typically occur as concretions, including pellets, nodules, and crusts. The saturation index for fluorapatite [$Ca_5(PO_4)_3F$] during phosphogenesis ranges from 5×10^{-8} to 2.5×10^{-7} g/L, under pH conditions of 7.1 to 7.8, Eh values between −0.1 and 3.0 (indicative of reducing environments), and temperatures from 5˚C to 20˚C [7] [11] [14]. These conditions are typically driven by microbial degradation of organic matter within sediments [9] [15]. Francolite formation is generally associated with suboxic to anoxic sediments, where phosphorus and carbon are released during microbial decomposition. The sedimentation rate also plays a critical role in controlling phosphogenesis [15].

Geological interest in phosphatic sediments has increased in recent decades due to their economic importance, particularly in the fertilizer industry, which consumes about 90% of global phosphate production [16] [17]. As a critical non-renewable resource for agriculture, phosphorites are essential for sustaining global food demand, with the production of synthetic fertilizers requiring around 150 million tons of phosphate annually [4]. Phosphates are also considered as a potential source for the rare earth elements [12].

Marine sediments have been known to contain phosphate nodules throughout geological time [18] [19]. In regions such as South Africa, Peru-Chile, and Baja California, organic-rich, diatomaceous sediments containing phosphate deposits are found [19]-[21]. These regions are characterized by exceptionally high levels of global bioproductivity [22]. Nonetheless, phosphates can also be found in low-productivity oceans, where the absorption of phosphorus was likely controlled by bacterial activity and organic matter [23]. Recent studies highlight the significance of bacterial sulfate reduction and sulfide oxidation as the most efficient microbial processes for concentrating and promoting apatite precipitation [3] [24]-[26]. According to [27] and [28], the late Proterozoic, Early Cambrian, Ordovician, Per-

mian, Late Cretaceous-Eocene, and Miocene were the most optimal times for phosphogenesis, while least favourable conditions characterized the Silurian, Devonian, Carboniferous, and Triassic. However, economically significant Devonian phosphates are rarely found, as indicated by examples in Iran [28] [29].

The Carboniferous-Permian marks a major phase of global phosphogenesis, with widespread deposits documented globally. The Permian is recognized as one of the key Phanerozoic periods of extensive phosphate accumulation [27] (**Figure 1**). The Phosphoria Formation in North America is a well-known example of Permian phosphorite development [30] [31]. Other notable Permian phosphorite deposits include Novaya Zemlya in Russia [32] and the Gufeng Formation on the Yangtze Platform in South China [33].

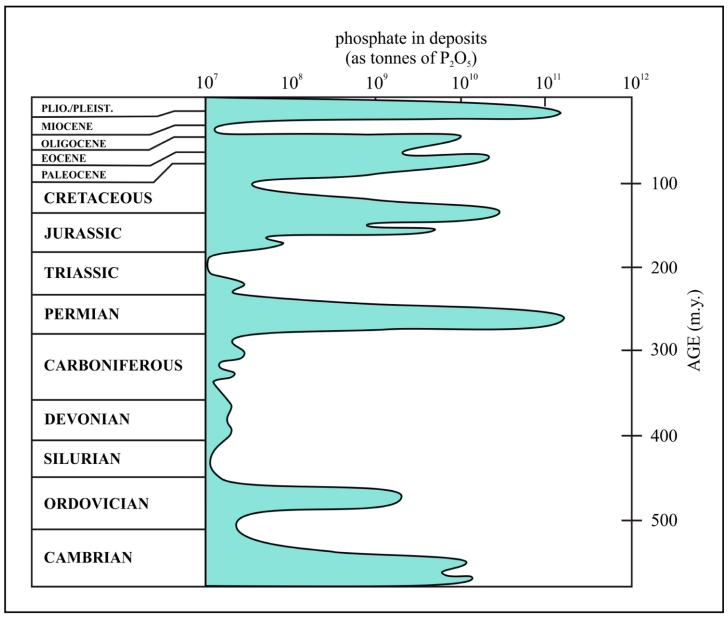

Figure 1. Estimated phosphate abundance (in metric tons of P_2O_5) across Phanerozoic deposits is illustrated using a histogram with fixed 25 million-year intervals. Notably, the P_2O_5 values are presented on a logarithmic scale (after Cook and McElhinny, 1979).

Despite a century of rigorous research, the mechanisms underlying their formation and the origin of their granular constituents remain subjects of ongoing debate. By accreting and bioerosioning phosphorite grains, microbial mediation activities in phosphogenic regions can contribute to phosphogenesis in either a beneficial or detrimental way [25] [34]-[42]. Marine phosphorites, which document a broad spectrum of depositional and diagenetic changes, are conventionally classified into two main types: granular and non-granular phosphorites [41] [43]. A range of phosphatic particles, such as phosphatised skeletal (for example, as fish bones, shark teeth, and bioclasts) and non-skeletal (for example, as nodules, coprolites, peloids, ooids, oncoids, aggregates, and lithoclasts) grains, make up granular phosphorites [44]. Due to our reliance on phosphate for fertilizers and various agricultural and chemical applications, these deposits are significant not only scientifically but also economically [7].

The Chamba basin in Himachal Pradesh, which represents the Tethyan domain in the northwest Himalaya, has been investigated since 1882, when McMahon, who was the first, surveyed the region and also established the earliest geological map [45] [46]. The Chamba region is part of a NW-SE trending longitudinal valley, located between the Zanskar and Dhauladhar ranges in the northeast and southwest, respectively. The Chamba region is part of a longitudinal valley with axial trace orienting NW-SE with gently southeastward-plunging axis that stretches over 100 km from Bhalesh to Bharmour via Kalhel with a width of approximately 20 km between its two limbs [47] [48]. In later years, contributions to the area's stratigraphy include [49]-[55].

The Salooni Formation of the Chamba basin is characterized by the presence of phosphorites, which occur as phosphate nodules. The Geological Survey of India was the first to find the phosphate nodules at the Chikoli bridge (32˚45 05 ″ N, 75˚59 40 ″E)—Bhatiyund (32˚43 ′N, 76˚04 ′E) area of Chamba district, Himachal Pradesh (**Figure 2**). Despite extensive investigation into the area, a thorough

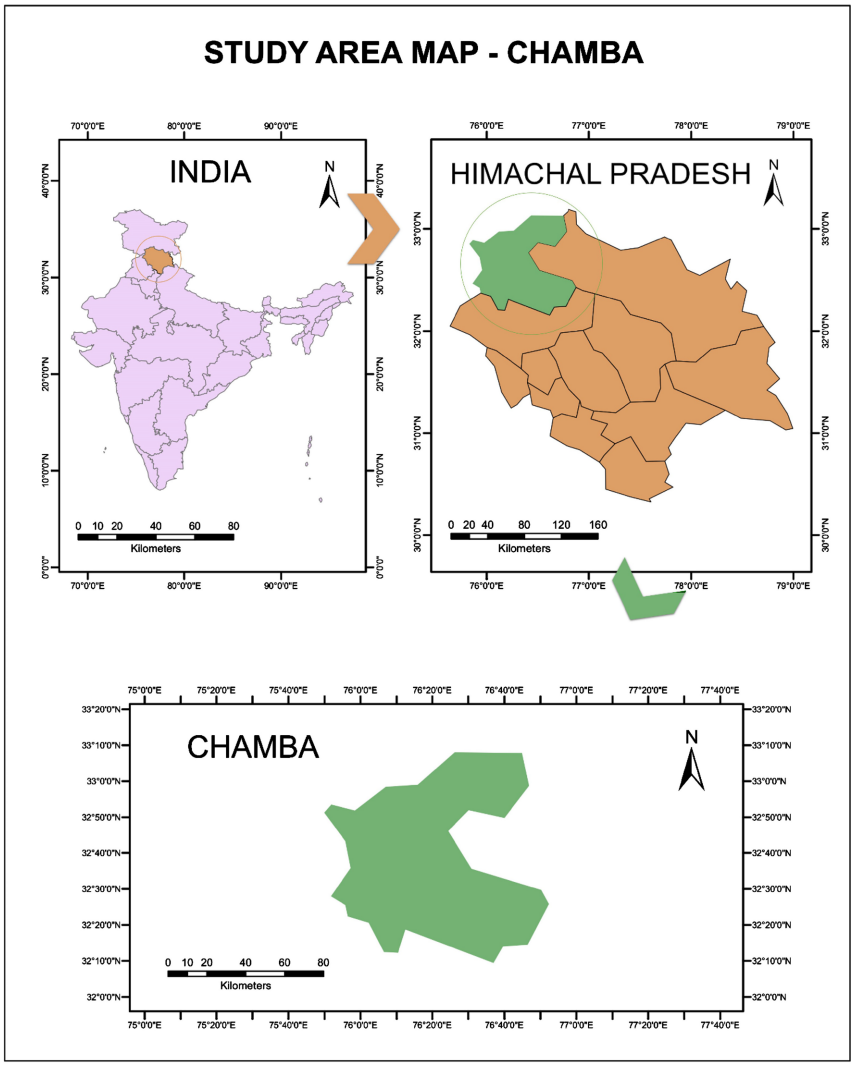

Figure 2. Location map of the Chamba district, Himachal Pradesh.

mineralogical assessment of the phosphate nodules in these deposits and a detailed explanation remains missing. The present investigation addresses the mineralogical features, distribution patterns, textures, and optical properties of phosphate-bearing minerals and associated gangue. It involves thin-section analysis, scanning electron microscopy (SEM), and X-ray diffraction (XRD) of phosphate nodules of the Chakoli bridge-Bhatiyund area of Chamba district, Himachal Pradesh to learn about their formation processes and the depositional environment of the basin.

Since no petrographic studies have previously been conducted in the study area, this paper focuses on the petrographic characteristics of phosphate nodules from the Chamba basin to better understand their genesis and depositional environment.

2. Geological Setup

Chamba nappe is located between the Chenab Normal Fault (CNF) to the NW and the Chail Thrust (also referred to as Panjal Thrust—[56] [57]) to the SW while having biostratigraphic similarities with the Tethys Himalaya Zone [58]. The Chamba sequence thrusts over the Lesser Himalayan succession to the southwest along the Chail Thrust (CT) and Higher Himalaya Crystallines (high-grade metamorphic rocks) to the northeast side along the CNF and is classified as the Chamba nappe (CN) [47] [59] [60]. The structure of the nappe represents two regional-scale synclinoriums named Chamba syncline and Tandi syncline, both exhibiting vergence in opposing directions. Vergence of the Chamba syncline is towards SW along the Chail Thrust [58] [61] [62] and the Tandi syncline is towards NE along the CNF [58] [63] [64]. Both the synclines possess several synforms and antiforms and were created when the succession of the nappe was tectonically folded into an overturned fold during the first phase of deformation [52] [65] [66]. This longitudinal valley (Chamba syncline) of axial trace orienting NW-SE with a gently southeastward-plunging axis stretches over 100 km from Bhalesh to Bharmour via Kalhel with a width of approximately 20 km between its two limbs and both limbs of which dip on the northeasterly side by an average of 30˚ [47] [48]. In the Churah area, the northwestern closure of the Chamba syncline suggests the plunging of the syncline is towards the NW side [47].

Chamba basin comprises roughly 8 to 10 kilometers of low-grade metasedimentary rocks arranged in a folded sequence, covering an area of nearly 140 km in length by 70 km average width [47] [58]. The study area is situated within the Chamba Basin of northwestern Himachal Pradesh, approximately 48 km north of Chamba city and about 90 km northeast of Dalhousie town. The rock formations of the Chamba syncline encompass very diverse lithologies in age ranging from the late Proterozoic era to the Triassic period [50] [54] [67]. The basement of the Chamba nappe sequence is the Salkhala group of rock formations which is predominantly exposed in the anticline's core on the northwest side of Chamba area as well as along the Panjal Thrust side limb of the Chamba syncline as a long narrow band that lies in the southwestern part [47] [53] [58].

In western Himachal Pradesh, the Salkhala group has been categorized into two units, namely the Bhalai Formation and the Chamba Formation. A set of concordant granitoid intrusions has been emplaced within the Salkhala Group of rocks, locally referred to as the Dhauladhar Granite, Dalhousie Granite, Mandi Granite, and Kersog Granite [68]. **Figure 3** and **Table 1** provide the geology and stratigraphy of the study area in Chamba region is described as follows: The Chamba Formation which forms the basal unit of the study area is succeeded by Manjir Formation, Katarigali Formation (Lower Salooni Formation/LSF), Saho Volcanics, Upper Salooni Formation and Kalhel Limestone—which occupies the core of the Chamba syncline.

The Chamba Formation consists of a thick succession comprising thinly bedded dark grey carbonaceous slates with limonitic encrustations, puckered lustrous phyllites, metapelitic schist, metasiltstones, metagreywacke and laminated to cross-bedded quartzites displaying strong flyschoid characteristics. The Manjir Formation unconformably overlies the Chamba formation, consists of grey and purple slates. Both the normal and inverted limbs of the formation have characteristic diamictite-bearing lithology and localized pebbly horizons. It comprises quartzite bands, pebble beds, shales, and interbedded limestone bands. The formation is sharply overlain by the Katarigali Formation. The Katarigali Formation (LSF) comprises dark grey to black carbonaceous pyritous slates (hard, compact, non-laminated, with poorly developed slaty cleavage) and thick, pyrite-disseminated phyllites, interbedded with quartzite, limestone, and graphite quartz-schist.

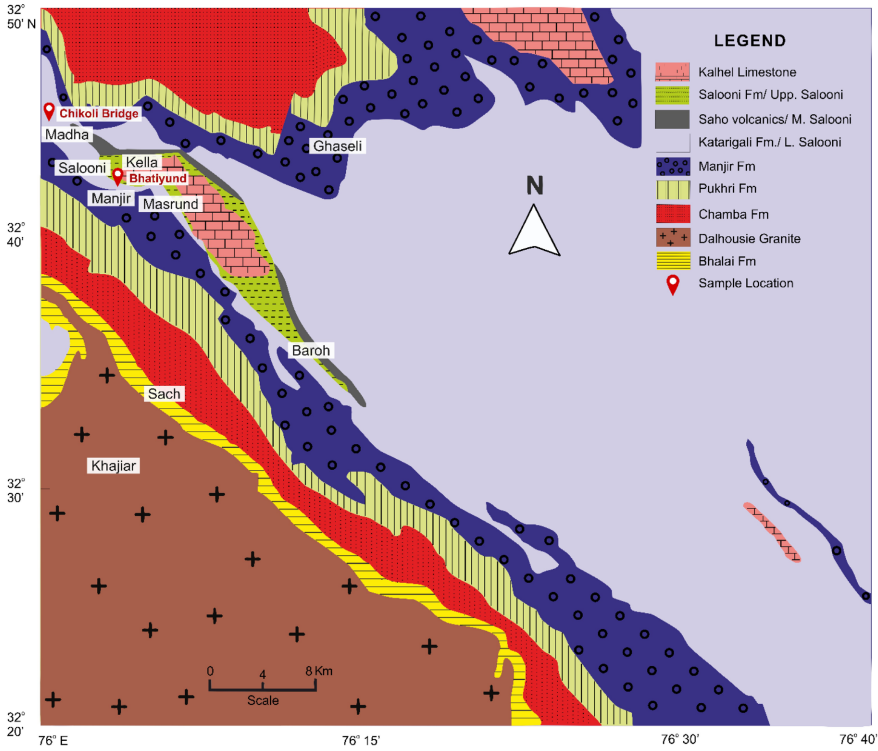

Figure 3. Generalized regional stratigraphic map of the Chamba region, Western Himalaya (after Sharma *et al.*, 2002).

Table 1. Stratigraphic sequence and lithological framework of the study area in Chamba region, Western Himalaya (modified after Srikantia and Bhargava, 1998).

Symbolic representation of formation	Formation	Age	Thickness (m)	Lithology
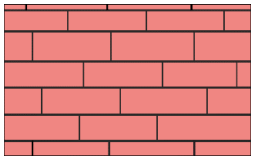	Kalhel Limestone	Lr. Triassic	400	Grey and yellow dolomitic limestones with interbedded white and grey orthoquartzites in the upper part and numerous stems and ossicles of crinoids in the lower part.
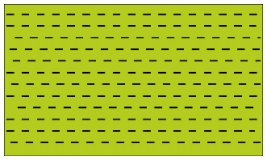	Upper Salooni	M. Permian to U. Permian	400	Limestones interbedded with grey calcareous slates/calcareous phyllites/quartzites.
	Saho Volcanics	M. Permian	10–50	Metavolcanics of basaltic and andesitic Composition.
	Katarigali (Lr. Salooni)	Up. Carbo. to M. Permian	800	Dark grey and carbonaceous pyritous slates, containing black phosphate nodules/siliceous crystalline limestone/carbonaceous phyllite/ phyllitic quartzites.
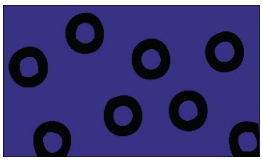	Manjir Conglomerate	Lr. Permian (Pande *et.al.* 2010)	1000	Grey and purple metamorphosed pebbly mud-stones paraconglomerates with intercalated bands of grey slates, consisting of conglomeratic flysch.
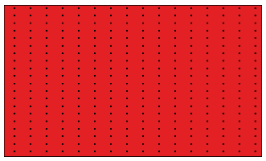	Chamba	M. Proterozoic	3500	Monotonous alteration of metagraywacke and slate, forming sandy flysch.

Within the phyllites pyrite commonly occurs as disseminations, stringers, and veins, while quartz as veins and pockets.

Phosphate nodules are confined only to the black carbonaceous slate unit of the Lower Salooni Formation (LSF) (**Figures 4(a)-(c)**) and occur parallel to both the cleavage and rock bedding. These nodules are dark grey to black, sub-rounded to oval in shape, and vary in size from 3 × 4 cm to 15 × 35 cm across. Phosphate nodules generally lack internal structures, although concentric layering may occasionally be observed. These nodules, sporadically distributed, exhibit conchoidal fracture and are often flattened due to tectonic compression (**Figures 5(a)-(c)**). Additionally, the nodules contain disseminations, streaks, and specks of pyrite. These nodules having P_2O_5 concentration ranging from 20% to 30% indicate

their economic importance [69].

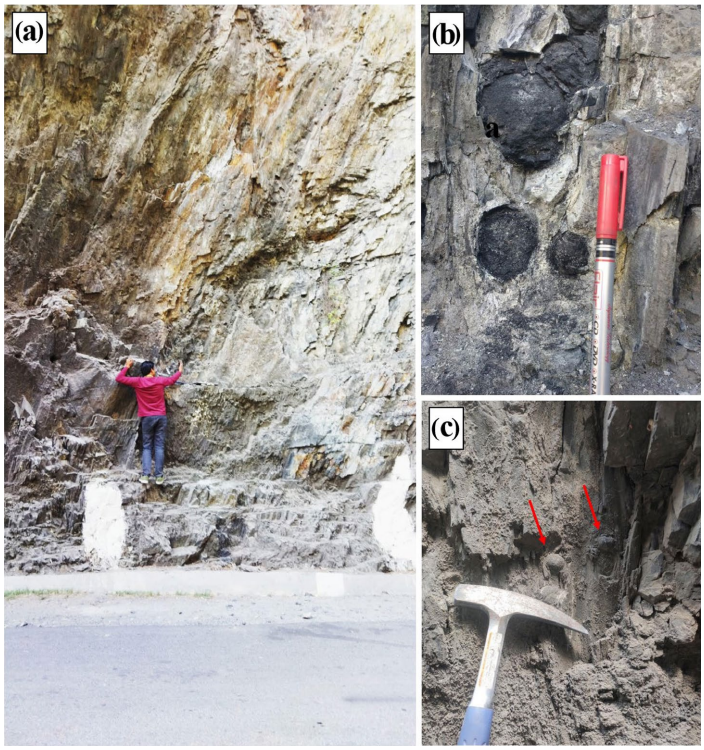

Figure 4. Representative field photographs of the studied outcrops. (a) Outcrop view of carbonaceous slate alongside the road at Chikoli bridge: man's height is 167 cm, (b) and (c) Nodule-bearing black carbonaceous slate of the Salooni Formation at the Chikoli bridge section. Red arrows mark the presence of nodules.

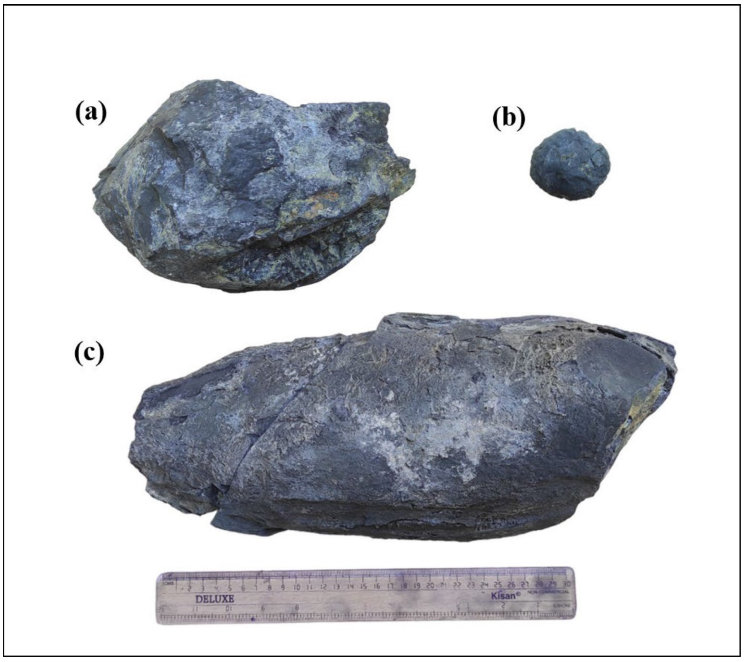

Figure 5. (a)-(c) Photograph of hand specimens of phosphate nodules retrieved from the study area.

Flows ranging from composition of basaltic to andesitic in the form of sills, and dykes (10 - 50 m thick) intrude the Salooni Formation (Lower and Upper Salooni) aligning with NW-SE foliation trends constitute the Saho Volcanics. These intrusive vary from light grey to dark greenish-grey in color, with cryptocrystalline to holocrystalline textures, and in amygdaloidal nature appear to be doleritic composition. The Upper Salooni Formation comprises interbedded grey slate, carbonaceous slate, calcareous phyllite, quartzite, and limestone and the presence of fossils including *Modiola lidarensis*, *Spiriferalla rajah*, and *Productus* sp. further corroborate its Permian age [51]. The Kalhel Formation (Triassic), the youngest stratigraphic unit in the area, comprises 400 m of interbedded crystalline limestone (variegated grey, bluish-grey, and pink) and dolomitic limestone (including crinoidal and cherty varieties), alongside calcareous phyllite, orthoquartzite, and shaly slate [70].

3. Methodology

Sampling was carried out from important locations of the area named as (1) near the Chikoli bridge, which is 8.5 km northwest of Salooni tehsil, and (2) at the Bhatiyund locality, which is about 13 km west of Salooni tehsil. Using a geological map and toposheet.map (Nos. 52 D/2 and 43P/13) of the examined area, 35 representative phosphate nodule samples were taken from the Chikoli bridge (32˚45'05" N, 75˚59'40" E) and the Bhatiyund outcrop (32˚43' N, 76˚04' E). Samples from several stratigraphic levels and horizons were systematically taken at regular intervals to minimize any sampling bias within the bed, if present, and to achieve an optimal range of nodule variation. Thin sections were prepared and examined with a polarizing microscope at various magnifications to determine their optical properties of mineral assemblages.

The samples were ground to a size of about 200 mesh to get distinct mineral diffraction patterns. Using a Shimadzu LabX XRD-6100 with a Cu-Kα radiation source (λ = 1.54), the mineralogy of the sample was analyzed by powder X-ray diffraction (XRD) to determine the type and distribution of crystalline phases present in powder samples with a scanning rate of 8 deg/min over a 2θ range of 10-65˚ at room temperature. The X-rays were generated at a voltage of 40 kV and a current of 30 mA. The JCPDS cards' X-ray identification charts and the PANalytical X'pert High Score Plus® software were utilized for data analysis.

The freshly broken surfaces of the samples were affixed to SEM stubs applying black carbon tape. The samples were then gold coated via a sputter coater and were subsequently analyzed using a scanning electron microscope (SEM) (JOEL JSM-6510, Japan) that included an EDX (energy dispersive X-ray) microanalyzer at the University Sophisticated Instruments Facility, AMU, Aligarh, to analyze the crystal morphology, shape, size, and characteristics of the mineral grains. The SEM images shown in this study were taken at various magnifications.

The methodology employed for the petrographic analysis of phosphate nodules is illustrated in a stepwise workflow diagram summarizing each procedural step (**Figure 6**).

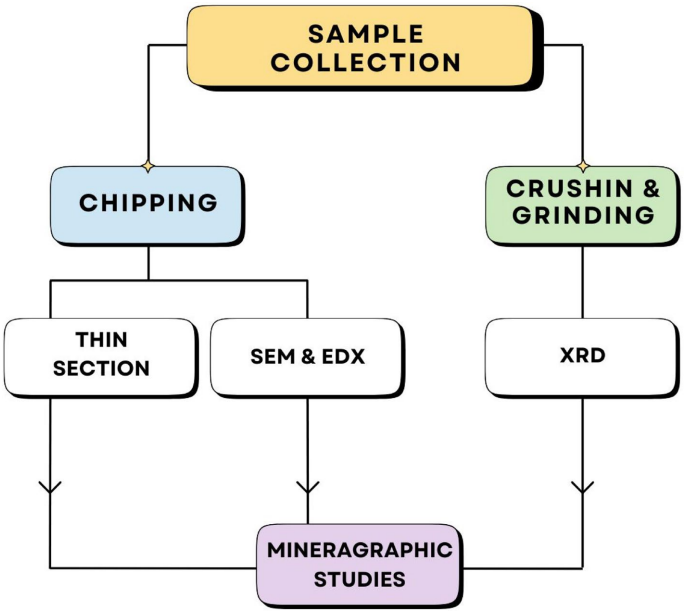

Figure 6. Workflow diagram outlining the stepwise procedure of the methodology used for petrographic study of phosphate nodules.

4. Results and Discussion

Microscopic examination reveals that phosphorites consist of phosphatic (principal), non-phosphatic grains and organic matter in smaller amounts. The phosphatic constituents occur as pellets, nodules, and apatite-rich matrix in the groundmass, predominantly composed of cryptocrystalline carbonate-fluorapatite (CFA), the primary phosphate mineral within the nodules. In contrast, microquartz, pyrite, dolomite and siliceous material represent the non-phosphatic constituents. In plane-polarized light, CFA appears dark brown, while under crossed nicols it exhibits a black, pseudoisotropic appearance, attributed to the aggregate polarization caused by its cryptocrystalline texture. The groundmass of structureless cryptocrystalline CFA contains well-rounded phosphate peloids dispersed throughout (**Figures 7(a)-(c)**). The presence of phosphatic pellets within the nodules suggests an early diagenetic origin, formed shortly below the sediment-water interface and is supported by the stable-isotopic study [9] [71]-[73]. Organic matter present in the phosphate nodules imparts a brown to brownish-black coloration. In areas where the organic content is higher, the color appears notably more intense (**Figure 7(b)**). Organic matter is broken down by microbes, which is usually associated with the reduction of nitrate ($NO3^{-}$) and sulphate ($SO4^{2-}$). This process releases labile phosphorus, and free sulphide which drives the precipitation of pyrite [74] [75]. It observed that in certain pellets within the nodules and phosphate material has been partially replaced by siliceous matrix (**Figures 7(a)-(c)**) with relict patches of the original phosphatic composition preserved in certain places (**Figure 7(c)**). Siliceous material has replaced the initial phosphate matrix of the nodules, forming a network-like structure (**Figure 7(d)** and **Figure 7(e)**). Replacement of phosphates by silica and pyrite shows a succes-

sion of post-depositional diagenetic changes [74] [76]. A few peloids appear as "phosphate envelopes"—grains with a phosphatic rim similar in composition to typical peloids, but with calcite cement filling the core. These uncommon structures are interpreted as the result of internal dissolution and subsequent calcite cementation (**Figure 7(f)**). The present work has been corroborated with the other workers like [2] [77]-[79].

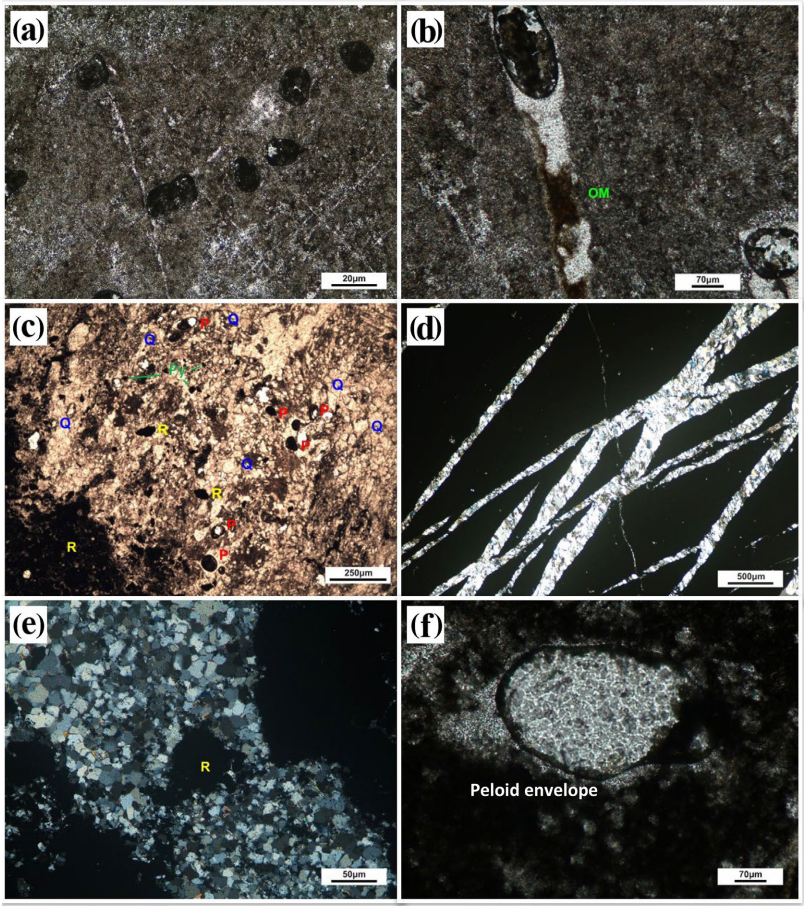

Figure 7. Photomicrographs of representative thin section of phosphate nodules under transmitted light microscopy. (a)-(c) Scattered phosphate peloids within the cryptocrystalline groundmass of CFA. Phosphate nodules exhibiting brown coloration due to the presence of organic material and showing partial silica replacement in some peloids; (d) and (e) Network-like replacement of the phosphate matrix by siliceous matter with some remnant matrix in the center of a vein; (f) Replacement of core of the peloid by calcitic material (CFA: Carbonate fluorapatite; OM: Organic matter; P: Peloid; R: Remnant phosphate matrix; Py: Pyrite; Q: Quartz).

CFA (also Francolite) and hydroxylapatite are the main constituents of the phosphate nodules while the latter is in major proportion were identified by sharp and well-defined diffraction peaks revealed in the X-ray diffraction (XRD) results. The other minor (also non-phosphatic) mineral phases contain quartz and kaolinite or chlorite (**Figures 8(a)-(c)**). Comparable results have been documented in phosphate nodules from Guizhou Province, South China [80].

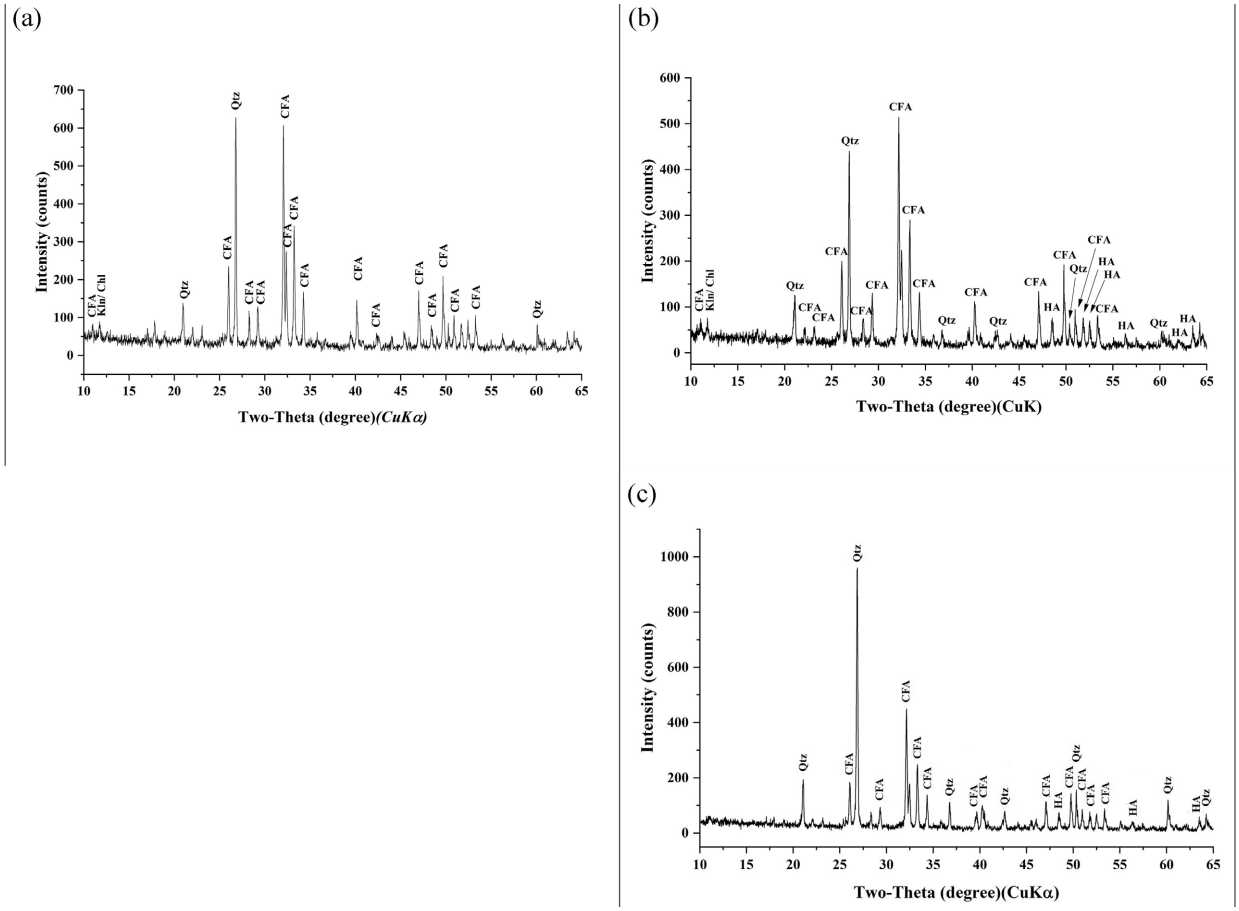

Figure 8. XRD spectra pattern showing presence of major and accessory minerals of phosphate nodules of the study area. (CFA: Carbonate fluorapatite; HA: Hydroxylapatite; Qtz: Quartz; Kln: Kaolinite; Chl: Chlorite).

Due to the exceptionally fine-grained character of CFA e.g. fabric, crystal dimensions, and crystal form, individual crystals in sedimentary phosphate rocks cannot be observed with a standard petrographic microscope. Scanning electron microscopy (SEM) analysis of phosphate nodules was conducted on freshly fractured surfaces to examine their internal texture. SEM observations reveal that the apatite crystals in semi-euhedral form with little erosion seen on the edges of the crystals indicate the recrystallization of CFA crystal (**Figure 9**). Crystalline apatite identified in the samples (**Figure 9**) may support to the claims of [81] and [82] that phosphates first precipitated as non-crystalline or slightly crystalline metastable phases before changing into crystalline apatite based on the level of fluorapatite supersaturation and the present findings support conclusions of [83]. In the photomicrograph successive stages of growth and crystallization within an apatite crystal exhibit (**Figure 10**) and these findings align with the findings published by [83]. A highly porous texture is formed by the aggregation of fine-grained phosphate crystals of micrometre scale, exhibiting predominantly equant granular and short-prismatic eucrystalline as seen in microstructure of CFA and the elemental composition of phosphate particles is further confirmed by EDX analysis (**Figure 11(a)** and **Figure 11(b)**). Basal sections of CFA appear as hexagonal prisms, forming a polygonal

ultrastructure composed of laminated or randomly arranged hexagonal apatite crystals (0.9 - 1.5 μm wide), which are either welded or retain their separate crystal morphology. [2] [84]-[86] came to similar conclusions, which also corroborate the current findings. In the examined samples, two modes of occurrence were identified: diagenetic replacement and direct precipitation. Diagenetic francolites display fibrous crystals with radial arrangements relative to the grain surface (**Figure 12**).

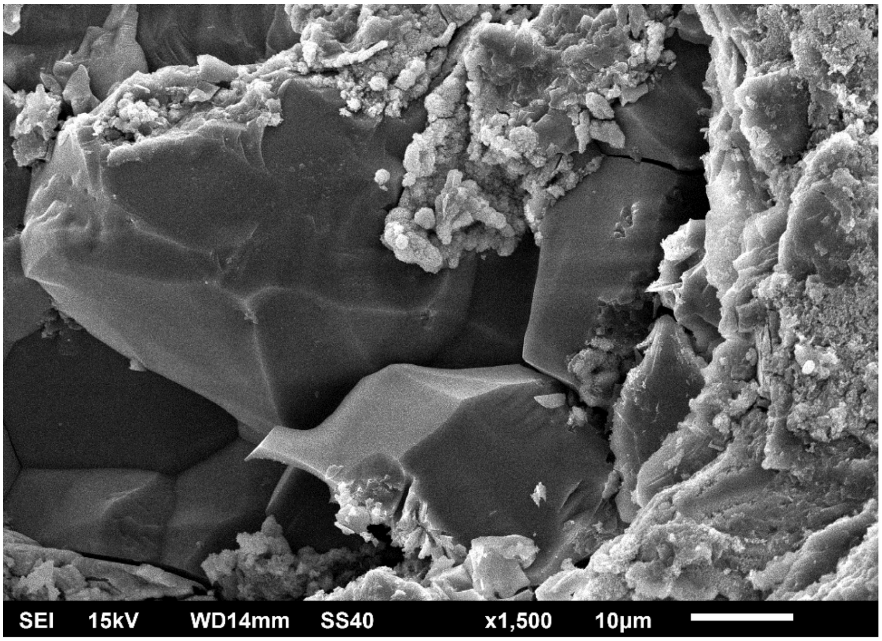

Figure 9. Scanning electron micrograph exhibiting semi-euhedral crystals indicating recrystallization of apatite crystals.

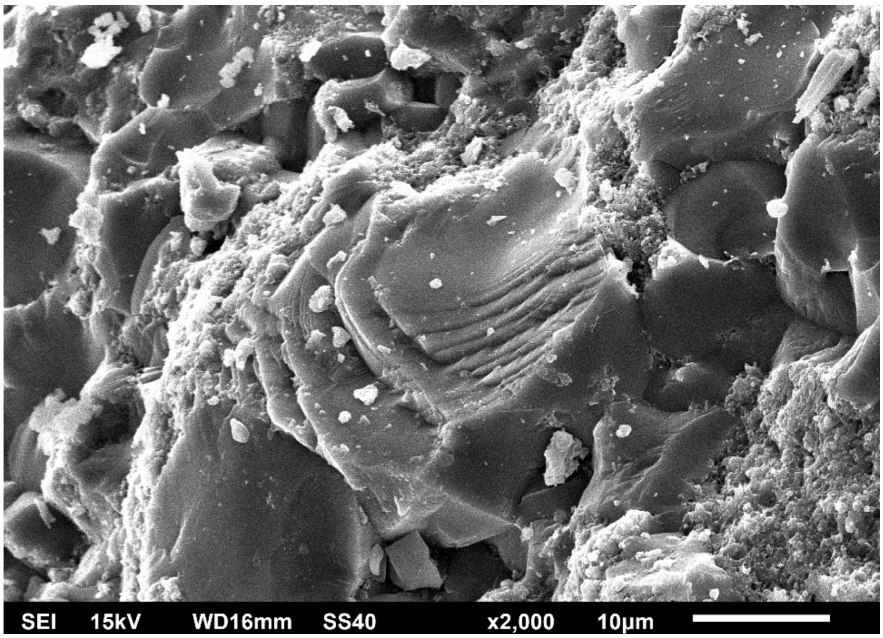

Figure 10. Scanning electron micrograph showing successive growth stages of an apatite crystal.

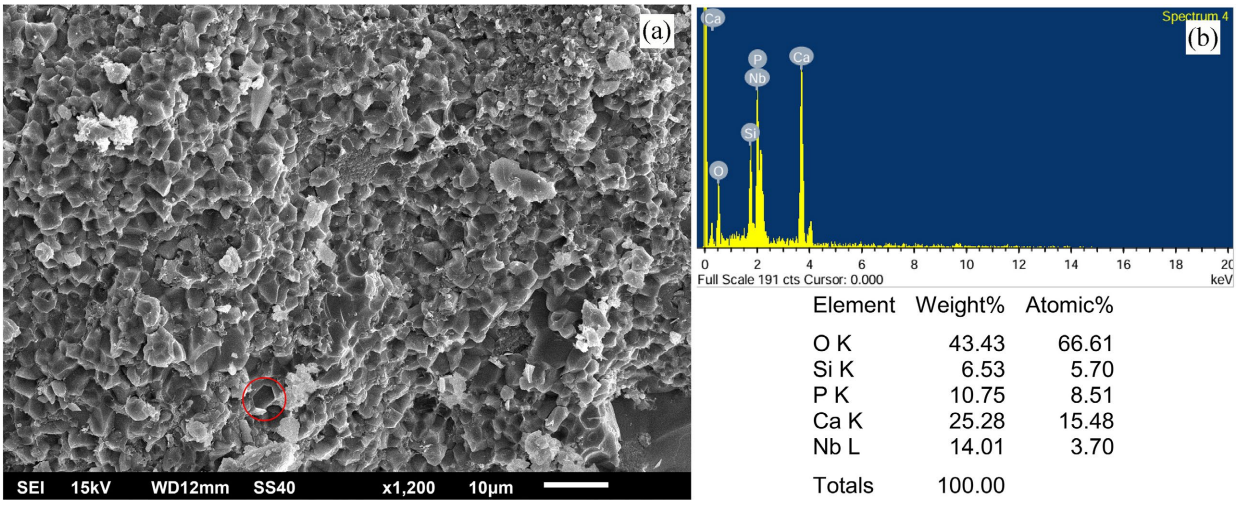

Figure 11. (a) Scanning electron micrographs of phosphate nodules showing porous texture formed by apatite crystals; (b) EDX spectrum indicating elemental composition. Red circle marks the basal section of CFA.

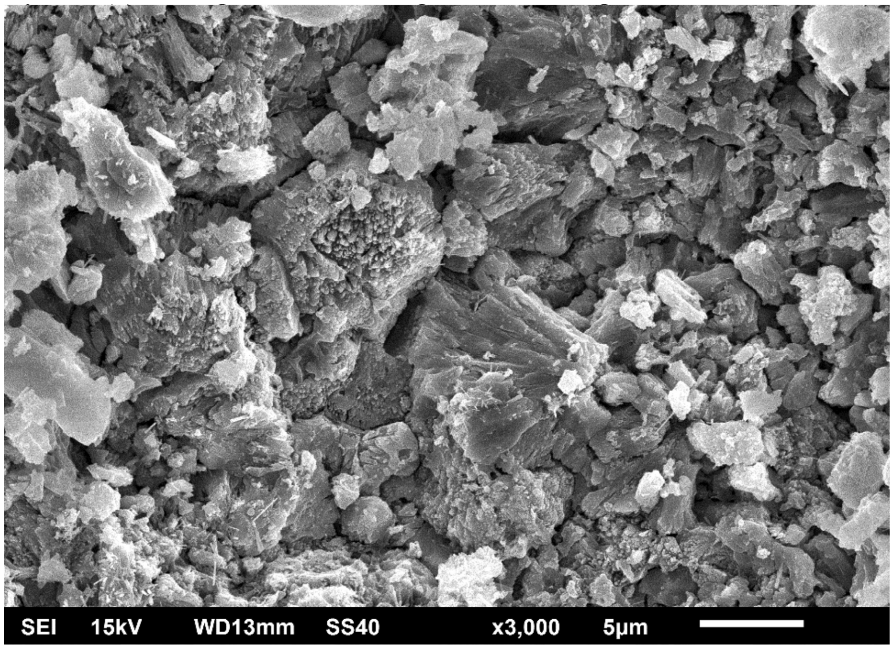

Figure 12. Scanning electron micrograph exhibiting radial growth structure of some acicular apatite crystals.

By contrast, authigenic francolites—formed via direct precipitation—are distinguished by large, well-developed euhedral crystals within micropores (**Figure 9**). The variation in crystallinity may be attributed to differences in algal assemblages, organic matter content, and pore-water chemistry, and is possibly more directly influenced by the rate of crystal growth or the presence of impurities. This explanation aligns with the work of [87] [88]. Quartz is present at the center which occurs on the surface of micro-structured globular phosphatized particles, accompanied by well-crystallized CFA particles and the elemental composition of quartz is further confirmed by EDX analysis (**Figure 13(a)** and **Figure 13(b)**). Platy crystals

appear as loosely arranged, euhedral to subhedral outlines, aligned face-to-face along their elongation, and is observed filling a microfracture between two CFA grains that may be either kaolinite or chlorite as kaolinite (7 Å mineral), cannot be distinguished from chlorite using XRD analysis when both minerals are present (**Figure 14**) and has been supported by other researchers including as [89]-[91].

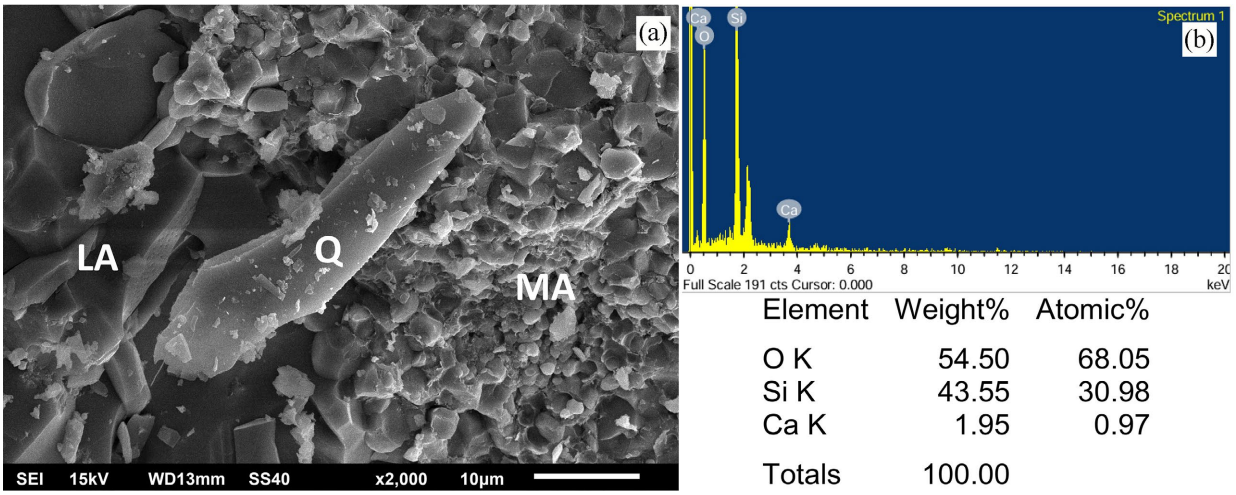

Figure 13. Scanning electron micrograph showing (a) quartz and variety of apatite crystals; (b) quartz is identified by the EDX analysis (LA: Large apatite crystal; Q: Quartz; MA: Micro-structured apatite).

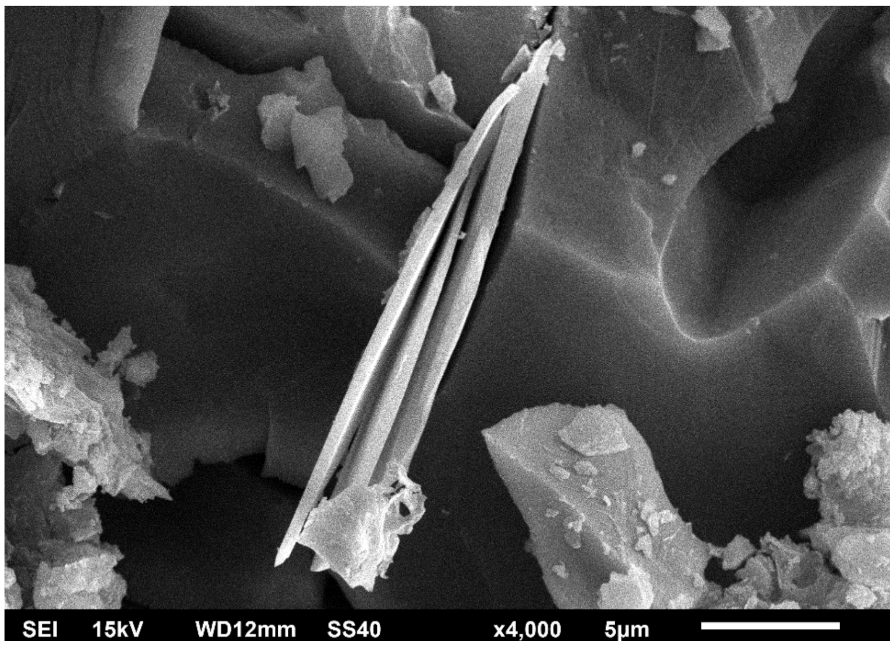

Figure 14. Scanning electron micrographs showing platy kaolinite or chlorite between adjacent apatite crystals.

5. Conclusions

The phosphate nodules of the Chikoli-Bhatiyund region in Chamba district are primarily hosted within the black carbonaceous slate of the Lower Salooni Formation.

It is concluded that carbonate fluorapatite (CFA) is the chief phosphate mineral, with quartz as the major gangue mineral, pyrite, carbonate, and clay as minor gangue constituents. Analytical methods including X-ray diffraction, thin-section petrography, and scanning electron microscopy along with EDX collectively reveal apatite crystals that are euhedral to subhedral and exhibit equant granular to prismatic forms, accompanied by a porous matrix and siliceous replacement textures occurring both within individual phosphate peloids and throughout the phosphate matrix as a network of silica veins. Disseminated pyrite and organic matter observed in the nodules suggest localized reducing conditions during diagenesis. Evidence of microbial filaments seen in SEM images supports the involvement of microorganisms which indicate the early diagenetic processes in phosphogenesis. Microfracture fillings by kaolinite/chlorite suggest that the phosphate-bearing sequences formed under conditions of intense chemical weathering of the continental landmass.

The mineral assemblages and replacement textures imply initial precipitation under shallow marine suboxic to anoxic conditions. The mutual replacement of phosphate by silica indicates the last stage of diagenesis and varying chemical conditions during burial. While these nodules are currently limited in distribution, their high phosphorus content underscores their potential as an alternative resource for fertilizer production.

The present study adds new insight into the genesis and mineral composition of phosphatic nodules within the Chamba Basin.

Acknowledgements

The first and third authors are thankful to the Chairperson, Department of Geology, and University Sophisticated Instruments Facility, Aligarh Muslim University, Aligarh, for providing the necessary facilities. Shamim A. Dar acknowledges the support of the HOD, Department of Geology, B.H.U., Varanasi, for providing the required facilities. Shamim A. Dar is highly thankful to the Anusandhan National Research Foundation (ANRF), Science and Engineering Research Board (SERB), Department of Science & Technology, and Government of India for a start-up research grant (M-14/0599; Sanction order no. SRG/2022/001478) and Seed Grant under Institutions of Eminence (IoE), Banaras Hindu University (BHU) (Dev. Scheme No. 6031) for financial assistance.

Conflicts of Interest

The authors declare that there are no conflicts of interest regarding the publication of this manuscript.

References

[1] Filippelli, G.M. (2011) Phosphate Rock Formation and Marine Phosphorus Geochemistry: The Deep Time Perspective. *Chemosphere*, **84**, 759-766. https://doi.org/10.1016/j.chemosphere.2011.02.019

[2] Dar, S.A., Khan, K.F., Khan, S.A., Khan, S. and Masroor Alam, M. (2014) Petro-Mineralogical Studies of the Paleoproterozoic Phosphorites in the Sonrai Basin, Lalitpur District, Uttar Pradesh, India. *Natural Resources Research*, **24**, 339-348. https://doi.org/10.1007/s11053-014-9260-x

[3] Crosby, C.H. and Bailey, J.V. (2012) The Role of Microbes in the Formation of Modern and Ancient Phosphatic Mineral Deposits. *Frontiers in Microbiology*, **3**, Article 241. https://doi.org/10.3389/fmicb.2012.00241

[4] Robb, L. (2020) Introduction to Ore-Forming Processes. Blackwell Science Ltd.

[5] Filippelli, G.M. (2008) The Global Phosphorus Cycle: Past, Present, and Future. *Elements*, **4**, 89-95. https://doi.org/10.2113/gselements.4.2.89

[6] Aubineau, J., Parat, F., Elghali, A., Raji, O., Addou, A., Bonnet, C., *et al.* (2022) Highly Variable Content of Fluorapatite-Hosted Coin the Upper Cretaceous/Paleogene Phosphorites (Morocco) and Implications for Paleodepositional Conditions. *Chemical Geology*, **597**, Article ID: 120818. https://doi.org/10.1016/j.chemgeo.2022.120818

[7] Knudsen, A.C. and Gunter, M.E. (2002) Sedimentary Phosphorites—An Example: Phosphoria Formation, Southeastern Idaho, U.S.A. *Reviews in Mineralogy and Geochemistry*, **48**, 363-389. https://doi.org/10.2138/rmg.2002.48.9

[8] Baturin, G.N. and Bezrukov, P.L. (1979) Phosphorites on the Sea Floor and Their Origin. *Marine Geology*, **31**, 317-332. https://doi.org/10.1016/0025-3227(79)90040-9

[9] Glenn, C., Föllmi, K., Riggs, S.R., *et al.* (1994) Phosphorus and Phosphorites: Sedimentology and Environments of Formation. *Eclogae Geologicae Helvetiae*, **87**, 747-788.

[10] Drummond, J.B.R., Pufahl, P.K., Porto, C.G. and Carvalho, M. (2015) Neoproterozoic Peritidal Phosphorite from the Sete Lagoas Formation (Brazil) and the Precambrian Phosphorus Cycle. *Sedimentology*, **62**, 1978-2008. https://doi.org/10.1111/sed.12214

[11] Boulemia, S., Hadji, R., Bouhlal, S., Hamed, Y., Besser, H. and Ncibi, K. (2023) Geological and Mineralogical Analysis of Phosphorites in the Jebel Dhyr Syncline, Eastern Algerian Atlas. *Mineralogia*, **54**, 89-104. https://doi.org/10.2478/mipo-2023-0010

[12] Dar, S.A., Khan, K.F., Mir, A.R., Komiya, T., Absar, N., Shuaib, M., *et al.* (2025) Geochemical and C-O Isotopic Study of ~2-1.9 Ga Phosphate-Bearing Marine Sedimentary Rocks of the Sonrai Formation, Bijawar Group, Lalitpur District, UP, India: Implications for Paleoredox, Paleoclimate, and Paleosalinity. *Geosystems and Geoenvironment*, **4**, Article ID: 100324. https://doi.org/10.1016/j.geogeo.2024.100324

[13] Follmi, K. (1996) The Phosphorus Cycle, Phosphogenesis and Marine Phosphate-Rich Deposits. *Earth-Science Reviews*, **40**, 55-124. https://doi.org/10.1016/0012-8252(95)00049-6

[14] Van Cappellen, P. and Berner, R.A. (1988) A Mathematical Model for the Early Diagenesis of Phosphorus and Fluorine in Marine Sediments; Apatite Precipitation. *American Journal of Science*, **288**, 289-333. https://doi.org/10.2475/ajs.288.4.289

[15] Zarasvandi, A., Fereydouni, Z., Pourkaseb, H., Sadeghi, M., Mokhtari, B. and Alizadeh, B. (2019) Geochemistry of Trace Elements and Their Relations with Organic Matter in Kuh-E-Sefid Phosphorite Mineralization, Zagros Mountain, Iran. *Ore Geology Reviews*, **104**, 72-87. https://doi.org/10.1016/j.oregeorev.2018.10.013

[16] Zapata, F. and Roy, R.N. (2004) Use of Phosphate Rocks for Sustainable Agriculture. *FAO Fertilizer and Plant Nutrition Bulletin*, **13**, 1-148.

[17] Cultrone, G., Anfuso, G. and Sebastián, E. (2008) Mineralogy of Miocene Phosphatic Nodules in SE Sicily (Italy). *Geological Quarterly*, **52**, 61.

[18] Ilyin, A.V. (1998) Rare-Earth Geochemistry of 'Old' Phosphorites and Probability of Syngenetic Precipitation and Accumulation of Phosphate1in Memory of Richard P. Sheldon. *Chemical Geology*, **144**, 243-256. https://doi.org/10.1016/s0009-2541(97)00134-4

[19] Jiang, S., Zhao, H., Chen, Y., Yang, T., Yang, J. and Ling, H. (2007) Trace and Rare Earth Element Geochemistry of Phosphate Nodules from the Lower Cambrian Black Shale Sequence in the Mufu Mountain of Nanjing, Jiangsu Province, China. *Chemical Geology*, **244**, 584-604. https://doi.org/10.1016/j.chemgeo.2007.07.010

[20] Veeh, H.H., Burnett, W.C. and Soutar, A. (1973) Contemporary Phosphorites on the Continental Margin of Peru. *Science*, **181**, 844-845. https://doi.org/10.1126/science.181.4102.844

[21] Schuffert, J.D., Jahnke, R.A., Kastner, M., Leather, J., Sturz, A. and Wing, M.R. (1994) Rates of Formation of Modern Phosphorite off Western Mexico. *Geochimica et Cosmochimica Acta*, **58**, 5001-5010. https://doi.org/10.1016/0016-7037(94)90227-5

[22] Walsh, J.J. (1981) A Carbon Budget for Overfishing off Peru. *Nature*, **290**, 300-304. https://doi.org/10.1038/290300a0

[23] O'Brien, G.W., Harris, J.R., Milnes, A.R. and Veeh, H.H. (1981) Bacterial Origin of East Australian Continental Margin Phosphorites. *Nature*, **294**, 442-444. https://doi.org/10.1038/294442a0

[24] Arning, E.T., Birgel, D., Brunner, B. and Peckmann, J. (2009) Bacterial Formation of Phosphatic Laminites off Peru. *Geobiology*, **7**, 295-307. https://doi.org/10.1111/j.1472-4669.2009.00197.x

[25] Hiatt, E.E., Pufahl, P.K. and Edwards, C.T. (2015) Sedimentary Phosphate and Associated Fossil Bacteria in a Paleoproterozoic Tidal Flat in the 1.85Ga Michigamme Formation, Michigan, Usa. *Sedimentary Geology*, **319**, 24-39. https://doi.org/10.1016/j.sedgeo.2015.01.006

[26] Al-Bassam, K. and Halodová, P. (2018) Fossil Bacteria in Cenomanian-Turonian Phosphate Nodules and Coprolites, Bohemian Cretaceous Basin, Czech Republic. *Annales Societatis Geologorum Poloniae*, **88**, 257-272. https://doi.org/10.14241/asgp.2018.009

[27] Cook, P.J. and McElhinny, M.W. (1979) A Reevaluation of the Spatial and Temporal Distribution of Sedimentary Phosphate Deposits in the Light of Plate Tectonics. *Economic Geology*, **74**, 315-330. https://doi.org/10.2113/gsecongeo.74.2.315

[28] Fröhlich, S. (2004) Phosphatic Black Pebbles and Nodules on a Devonian Carbonate Shelf (Anti-Atlas, Morocco). *Journal of African Earth Sciences*, **38**, 243-254. https://doi.org/10.1016/j.jafrearsci.2004.01.005

[29] Movahhed, A., Samimi, N. and Ghasemipur, R. (1968) Upper Devonian Phosphate. Recent Phosphate Discoveries in Iran. *Report, Geological Survey of Iran*, **10**, 13-55.

[30] Sheldon, R., Maughan, E. and Cressman, E. (1967) Sedimentation of Rocks of Leonard (Permian) Age in Wyoming and Adjacent States. *The Journal of Geology*, **110**, 1-13.

[31] Henderson, C.M., Bamber, E.W., Richards, B.C., Higgins, A.C. and McGugan, A. (1993) Permian. In: Stott, D.F. and Aitken, J.D., Eds., *Sedimentary Cover of the Craton in Canada*, Geological Society of America, 272-293. https://doi.org/10.1130/dnag-gna-d1.272

[32] Sobolev, N.N. and Nakrem, H.A. (1996) Middle Carboniferous-Lower Permian Conodonts of Novaya Zemlya. Norsk Polarinstitutt, Oslo.

[33] Kametaka, M., Takebe, M., Nagai, H., Zhu, S. and Takayanagi, Y. (2005) Sedimentary

Environments of the Middle Permian Phosphorite-Chert Complex from the Northeastern Yangtze Platform, China; the Gufeng Formation: A Continental Shelf Radiolarian Chert. *Sedimentary Geology*, **174**, 197-222. https://doi.org/10.1016/j.sedgeo.2004.12.005

[34] Dahanayake, K. and Krumbein, W.E. (1985) Ultrastructure of a Microbial Mat-Generated Phosphorite. *Mineralium Deposita*, **20**, 260-265. https://doi.org/10.1007/bf00204283

[35] Reimers, C., Kastner, M. and Garisson, R. (1990) The Role of Bacterial Mats in Phosphate Mineralization with Particular Reference to the Monterey Formation. In: Burnett, W.C. and Riggs, S.R., Eds., *Phosphate Deposits of the World*, Cambridge University Press, 300-311.

[36] Krajewski, K., Vancappellen, P., Trichet, J., Kuhn, O., Lucas, J., Martinalgarra, A., Prévôt, L., Tewari, V., Gaspar, L. and Knight, R. (1994) Biological Processes and Apatite Formation in Sedimentary Environments. *Eclogae Geologicae Helvetiae*, **87**, 701-745.

[37] Trappe, J. (1998) Phanerozoic Phosphorite Depositional Systems: A Dynamic Model for a Sedimentary Resource System. Springer.

[38] Schulz, H.N. and Schulz, H.D. (2005) Large Sulfur Bacteria and the Formation of Phosphorite. *Science*, **307**, 416-418. https://doi.org/10.1126/science.1103096

[39] Dornbos, S.Q. (2010) Phosphatization through the Phanerozoic. In: Allison, P.A. and Bottjer, D.J., Eds., *Taphonomy*, Springer, 435-456. https://doi.org/10.1007/978-90-481-8643-3_12

[40] Bailey, J.V., Corsetti, F.A., Greene, S.E., Crosby, C.H., Liu, P. and Orphan, V.J. (2013) Filamentous Sulfur Bacteria Preserved in Modern and Ancient Phosphatic Sediments: Implications for the Role of Oxygen and Bacteria in Phosphogenesis. *Geobiology*, **11**, 397-405. https://doi.org/10.1111/gbi.12046

[41] Salama, W., Khirekesh, Z., Amini, A. and Bafti, B.S. (2018) Diagenetic Evolution of the Upper Devonian Phosphorites, Alborz Mountain Range, Northern Iran. *Sedimentary Geology*, **376**, 90-112. https://doi.org/10.1016/j.sedgeo.2018.08.001

[42] Föllmi, K.B. (2016) Sedimentary Condensation. *Earth-Science Reviews*, **152**, 143-180. https://doi.org/10.1016/j.earscirev.2015.11.016

[43] Pufahl, P.K., Grimm, K.A., Abed, A.M. and Sadaqah, R.M.Y. (2003) Upper Cretaceous (Campanian) Phosphorites in Jordan: Implications for the Formation of a South Tethyan Phosphorite Giant. *Sedimentary Geology*, **161**, 175-205. https://doi.org/10.1016/s0037-0738(03)00070-8

[44] Slansky, M. (1986) Geology of Sedimentary Phosphates. https://www.osti.gov/biblio/6495412

[45] McMahon, C.A. (1883) Some Notes on the Geology of Chamb. *Records of the Geological Survey of India*, **16**, 35-42.

[46] Pande, A., Bhattacharya, D., Jha, N., Misra, R. and Chandra, S. (2004) Discovery of Early Permian Palynomorphs from the Manjir Formation, Chamba District, Himachal Pradesh. *Geological Society of India*, **63**, 665-669.

[47] Thakur, V.C. (1998) Structure of the Chamba Nappe and Position of the Main Central Thrust in Kashmir Himalaya. *Journal of Asian Earth Sciences*, **16**, 269-282. https://doi.org/10.1016/s0743-9547(98)00011-7

[48] Sharma, B.K. and Bhola, A.M. (2005) Kink Bands in the Chamba Region, Western Himalaya, India. *Journal of Asian Earth Sciences*, **25**, 513-528. https://doi.org/10.1016/j.jseaes.2004.05.003

[49] Fuchs, G. and Gupta, V. (1971) Palaeozoic Stratigraphy of Kashmir, Kishtwar and Chamba (Panjab Himalayas). *Verhandlungen der Geologischen Bundesanstalt*, **1**, 68-97.

[50] Rattan, S. (1973) Stratigraphy and Sedimentation of the Chamba Area, Western Himachal Pradesh. *Himalayan Geology*, **3**, 231-248.

[51] Datta, R. and Bhattcharyya, D. (1975) Marine Fossils from Salooni Formation, Chamba District, Himachal Pradesh. *Miscellaneous Publications, Geological Survey of India*, **24**, 59-64.

[52] Thakur, V.C. and Tandon, S.K. (1976) Significance of Pebble and Mineral Lineation in the Chamba Syncline of Punjab Himalaya, Himachal Pradesh, India. *Geological Magazine*, **113**, 141-149. https://doi.org/10.1017/s0016756800036438

[53] Srikantia, S. and Bhargava, O. (1998) Geology of Himachal Pradesh. GSI Publications, 262-265.

[54] Agarwal, G. and Kumar, B. (2004) Status of Chamba Formation, Chamba District, HP. *Records of the Geological Survey of India*, **136**, 111-113.

[55] Bhargava, O. (2008) Palaeozoic Successions of the Indian Plate. *Memoirs of the Geological Survey of India*, **74**, 209-244.

[56] Fuchs, G. (1975) Contributions to the Geology of the North-Western Himalayas. Geologische Bundesanstalt, Wien.

[57] Thakur, V.C. (1981) An Overview of Thrusts and Nappes of Western Himalaya. *Geological Society, London, Special Publications*, **9**, 381-392. https://doi.org/10.1144/gsl.sp.1981.009.01.35

[58] Singh, K. (2011) Opposite Vergent Synclines on the Flanks of a Large-Scale Box Fold in the Chamba-Lahaul Region, Northwest Himalaya, India. *International Journal of Earth Sciences*, **101**, 997-1008. https://doi.org/10.1007/s00531-011-0707-6

[59] Thakur, V.C. (1992) Geology of Western Himalaya. *Physics and Chemistry of the Earth*, **19**, 363.

[60] Rautela, P. and Thakur, V. (1992) Structural Analysis of the Panjal Thrust Zone, Himachal Himalaya, India. *Journal of Himalayan Geology*, **3**, 195-207.

[61] Singh, K. and Thakur, V.C. (1989) Strain Analysis in a Part of the Chamba Syncline Using Deformed Quartz Pebbles in Chamba Region of Northwestern Himalaya. *Journal Geological Society of India*, **33**, 140-149. https://doi.org/10.17491/jgsi/1989/330204

[62] Singh, K. (1993) Reverse and Oblique Slip Movement along the Chamba Thrust, North-West Himalaya: Implication for Tectonic Evolution. *Journal of the Himalayan Geology*, **4**, 143-148.

[63] Rawat, B. (1988) Lithostratigraphy and Structure of the Central Crystallines and the Phanerozoic Metasedimentaries of the Lahaul and Bharmour Regions of Himachal in North Western Himalaya. *Publications of the Centre for Advanced Studies in Geology*, **3**, 97-111.

[64] Vannay, J. and Steck, A. (1995) Tectonic Evolution of the High Himalaya in Upper Lahul (NW Himalaya, India). *Tectonics*, **14**, 253-263. https://doi.org/10.1029/94tc02455

[65] Gansser, A. (1964) Geology of the Himalayas. Interscience Publishers, 289.

[66] Datta, R.K. and Singh, S. (1975) Progress Report on the Geology of Parts of Chamba District, Himachal Pradesh (Field Season 1972-73). Geological Survey of India.

[67] Sharma, B.K. and Bhola, A.M. (2004) Microstructures of Co-Axially Folded Vein Seg-

ments and Crenulation Cleavage: Evidence for Dissolution Phenomena in the Chamba Thrust Sheet, Western Himalayas. *Episodes*, **27**, 119-124. https://doi.org/10.18814/epiiugs/2004/v27i2/006

[68] Kumar, R. (2022) Fundamentals of Historical Geology and Stratigraphy of India. New Age International Private Limited.

[69] Srivastava, R.N. (1969) A Note on Preliminary Investigation for Phosphorite in the Chamba District, Himachal Pradesh (Field Season 1968-69). Geological Survey of India.

[70] Lahoti, S., Kisley Kumud, K., Guota, Y. and Jain, A. (2017) Tectonics of the Chamba Nappe, NW Himalaya and Its Regional Implications. *Italian Journal of Geosciences*, **136**, 50-63. https://doi.org/10.3301/ijg.2015.39

[71] Al-Bassam, K.S. (1980) Carbon and Oxygen Isotopic Composition of Some Marine Sedimentary Apatites from Iraq. *Economic Geology*, **75**, 1231-1233. https://doi.org/10.2113/gsecongeo.75.8.1231

[72] Piper, D.Z. and Kolodny, Y. (1987) The Stable Isotopic Composition of a Phosphorite Deposit: $\delta^{13}C$, $\delta^{34}S$, and $\delta^{18}O$. *Deep Sea Research Part A. Oceanographic Research Papers*, **34**, 897-911. https://doi.org/10.1016/0198-0149(87)90044-6

[73] Glenn, C.R. and Arthur, M.A. (1988) Petrology and Major Element Geochemistry of Peru Margin Phosphorites and Associated Diagenetic Minerals: Authigenesis in Modern Organic-Rich Sediments. *Marine Geology*, **80**, 231-267. https://doi.org/10.1016/0025-3227(88)90092-8

[74] Rullkötter, J. (2006) Organic Matter: The Driving Force for Early Diagenesis. In: Schulz, H.D. and Zabel, M., Eds., *Marine Geochemistry*, Springer-Verlag, 125-168. https://doi.org/10.1007/3-540-32144-6_4

[75] Qiu, H., Feng, L., Chu, X., Li, L., Zhang, X. and Li, J. (2022) Genesis of Silica-Phosphatic Nodules with Small Shelly Fossils Preserved in the Lowermost Cambrian of South China. *Acta Geologica Sinica—English Edition*, **96**, 1294-1307. https://doi.org/10.1111/1755-6724.14924

[76] Brookfield, M.E., Hemmings, D.P. and Van Straaten, P. (2009) Paleoenvironments and Origin of the Sedimentary Phosphorites of the Napo Formation (Late Cretaceous, Oriente Basin, Ecuador). *Journal of South American Earth Sciences*, **28**, 180-192. https://doi.org/10.1016/j.jsames.2009.02.004

[77] Zoungrana, J., Sorgho, B., Bakouan, C., Sawadogo, S., Ouedraogo, R.D., Guel, B., *et al.* (2024) Mineralogical Study of Phosphate Rocks by Quantitative Rietveld Refinement. *Open Ceramics*, **18**, Article ID: 100567. https://doi.org/10.1016/j.oceram.2024.100567

[78] Shuaib, M., Khan, K.F., Khan, S. and Dar, S.A. (2019) Petromineralogical Studies of Late Paleocene-Middle Eocene Phosphate Nodules in the Subathu Basin of Solan District, Himachal Pradesh. *Mining, Metallurgy & Exploration*, **36**, 879-888. https://doi.org/10.1007/s42461-019-0082-6

[79] Kidder, D.L. (1985) Petrology and Origin of Phosphate Nodules from the Midcontinent Pennsylvanian Epicontinental Sea. *SEPM Journal of Sedimentary Research*, **55**, 809-816. https://doi.org/10.1306/212f880a-2b24-11d7-8648000102c1865d

[80] Ye, Y., Wang, H., Wang, X., Zhai, L., Wu, C. and Zhang, S. (2020) Elemental Geochemistry of Lower Cambrian Phosphate Nodules in Guizhou Province, South China: An Integrated Study by LA-ICP-MS Mapping and Solution ICP-MS. *Palaeogeography, Palaeoclimatology, Palaeoecology*, **538**, Article ID: 109459. https://doi.org/10.1016/j.palaeo.2019.109459

[81] Cappellen, P.V. and Berner, R.A. (1991) Fluorapatite Crystal Growth from Modified

Seawater Solutions. *Geochimica et Cosmochimica Acta*, **55**, 1219-1234. https://doi.org/10.1016/0016-7037(91)90302-l

[82] Rao, V.P., Hegner, E., Naqvi, S.W.A., Kessarkar, P.M., Ahmad, S.M. and Raju, D.S. (2008) Miocene Phosphorites from the Murray Ridge, Northwestern Arabian Sea. *Palaeogeography*, *Palaeoclimatology*, *Palaeoecology*, **260**, 347-358. https://doi.org/10.1016/j.palaeo.2007.12.003

[83] Sefik Imamoglu, M., Nathan, Y., Çoban, H., Soudry, D. and Glenn, C. (2008) Geochemical, Mineralogical and Isotopic Signatures of the Semikan, West Kasrık "Turkish" Phosphorites from the Derik-Mazıdağı-Mardin Area, SE Anatolia. *International Journal of Earth Sciences*, **98**, 1679-1690. https://doi.org/10.1007/s00531-008-0332-1

[84] Zanin, Y.N., Gilinskaya, L.G., Krasil'nikova, N.A., Krivoputskaya, L.M., Mirtov, Y.V. and Stolpovskaya, V.N. (1985) Calcium Phosphates in Phosphorites of Different Types. *International Geology Review*, **27**, 1212-1229. https://doi.org/10.1080/00206818509466496

[85] Sánchez-Navas, A. and Martín-Algarra, A. (2001) Genesis of Apatite in Phosphate Stromatolites. *European Journal of Mineralogy*, **13**, 361-376. https://doi.org/10.1127/0935-1221/01/0013-0361

[86] Knight, R.I. (1999) Phosphates and Phosphogenesis in the Gault Clay (Albian) of the Anglo-Paris Basin. *Cretaceous Research*, **20**, 507-521. https://doi.org/10.1006/cres.1999.0163

[87] Ece, O.I. (1990) Geochemistry and Occurrence of Authigenetic Phosphate Nodules from the Desmoinesian Cyclic Excello Epeiric Sea of the Midcontinent, USA. *Marine and Petroleum Geology*, **7**, 298-312. https://doi.org/10.1016/0264-8172(90)90007-4

[88] Lepland, A. and Bailey, J. (2016) Geochemistry, Microstructure and Origin of Recent Phosphorites on the Namibian Margin. https://core.ac.uk/download/pdf/187733243.pdf

[89] Zanin, Y.N., Zverev, K.V. and Solotchina, E.P. (1990) Clay Minerals and Phosphorite Genesis in the Upper Cretaceous of the Northern Siberian Platform. *Geological Society*, *London*, *Special Publications*, **52**, 223-235. https://doi.org/10.1144/gsl.sp.1990.052.01.16

[90] Keller, W.D. (1978) Classification of Kaolins Exemplified by Their Textures in Scan Electron Micrographs. *Clays and Clay Minerals*, **26**, 1-20. https://doi.org/10.1346/ccmn.1978.0260101

[91] Kadır, S., Külah, T., Eren, M., Önalgıl, N. and Gürel, A. (2014) Mineralogical and Geochemical Characteristics and Genesis of the Gülzelyurt Alunite-Bearing Kaolinite Deposit within the Late Miocene Gödeles Ignimbrite, Central Anatolia, Turkey. *Clays and Clay Minerals*, **62**, 477-499. https://doi.org/10.1346/ccmn.2014.0620603